J|A|C|S ARTICLES

Published on Web 04/24/2009

Octahedral $HSiCl_3$ and $HSiCl_2Me$ Adducts with Pyridines

Gerrit W. Fester,[†] Jörg Wagler,[†] Erica Brendler,[‡] Uwe Böhme,[†] Daniela Gerlach,[†] and Edwin Kroke*,[†]

Institut für Anorganische Chemie and Institut für Analytische Chemie, TU Bergakademie Freiberg, Leipziger Strasse 29, 09596 Freiberg, Germany

Received February 18, 2009; E-mail: edwin.kroke@chemie.tu-freiberg.de

Abstract: Stable solid adducts of substituted pyridines (Rpy) with $HSiCl_3$ and $HSiCl_2Me$ were prepared in high yields under aprotic and anaerobic conditions at room temperature. The octahedral complexes of $HSiCl_3$ underwent dismutation reactions in polar solvents. In contrast, the $HSiCl_2Me(Rpy)_2$ adducts were not susceptible to dismutation under comparable conditions, but they tended to dissociate more easily because of the reduced Lewis acidity of $HSiCl_2Me$ relative to $HSiCl_3$. The bonding between silicon and its surrounding ligands is highly ionic, as can be seen from QTAIM and charge distribution analyses. ^{29}Si CP/MAS spectra in combination with quantum-chemical calculations show that the lowest shielding is along the Cl−Si−Cl axis. The other two components of the shielding tensor are oriented along the N−Si−N and H−Si−Cl/Me axes. It is known that many reactions of (hydrido)chlorosilanes are catalyzed by pyridine bases. Therefore, the results presented here provide a basis for better control of these reactions, especially chlorine substitution and hydrosilylation.

Introduction

Trichlorosilane is one of the most important molecular silicon compounds, as it plays a crucial role in the process of producing ultrapure silicon (the Siemens process). Currently, several companies are strongly expanding their production capacities because of the rapidly increasing demand for solar-grade silicon.[1] Furthermore, an important industrial route to monosilane (SiH_4), which is a precursor for the production of high-purity silicon films, including thin-film solar cells, is based on the dismutation of trichlorosilane, $HSiCl_3$.[2] In addition to this prominent role in photovoltaic technology, trichlorosilane is used as a starting material for numerous organosilicon compounds since it is transformed into useful derivatives via hydrosilylation and/or chlorine substitution. Methylchlorosilanes, such as methyldichlorosilane, $HSiCl_2Me$, which are usually obtained by the so-called "direct process" or Müller−Rochow synthesis, are also produced on very large scales for the preparation of various organometallic silicon compounds, including siloxanes and silicones.[3]

Hypercoordinated $HSiCl_2Me$ adducts have not been described to date, and trichlorosilane adducts are very scarcely encountered in the literature. In the 1960s, Campell-Ferguson and Ebsworth[4] reported the reaction of *N*,*N*,*N*′,*N*′-tetramethylethylenediamine (tmeda) with $SiHCl_3$ in a 1:1 ratio to yield (tmeda)$SiHCl_3$ (eq 1): The poor solubility of the reaction products indicated

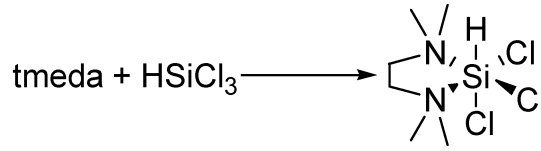

(1)

polymeric or ionic structures.[4] X-ray diffraction analysis, however, revealed the monomeric structure of the complex.[5] In addition to the sole Lewis base adduct formation, dismutation reactions of the hydridochlorosilanes have been described. Hensen and co-workers reported the first 1:2 adduct of trichlorosilane and pyridine (py). The enhanced reactivity of the complex, however, did not allow for slow crystallization and single-crystal X-ray diffraction analysis of this compound. As reported by Wannagat et al.,[6] $HSiCl_3(py)_2$ decomposes upon treatment with polar solvents (under H vs Cl redistribution and the formation of H_2SiCl_2, $SiCl_4$, and products thereof, as discussed below). In a more recent report, Fleischer et al.[7] described another example of such dismutation reactions: bis(dichlorosilyl)amine (in chloroform solution) reacts with substituted pyridines (Rpy) to yield H_3SiCl, H_2SiCl_2, and $HSiCl_3$.

As a consequence of our work on octahedral adducts of dichlorosilane with Rpy,[8] we also investigated the formation

[†] Institut für Anorganische Chemie, TU Bergakademie Freiberg.
[‡] Institut für Analytische Chemie, TU Bergakademie Freiberg.

(1) For example, see: (a) Voith, M. *Chem. Eng. News* **2008**, *86* (23), 13. (b) Tremblay, J.-F. *Chem. Eng. News* **2008**, *86* (28), 11–16. (c) Voith, M. *Chem. Eng. News* **2008**, *86* (36), 9. (d) Voith, M. *Chem. Eng. News* **2008**, *86* (51), 8. (e) Fishman, O. S. *Adv. Mater. Processes* **2008**, *166*, 39–40.
(2) For example, see: (a) Sonnenschein, R. Müller, A. Sill, T. Gölz, A.; Beyer, C.; Adler, P. In *Silicon for the Chemical Industry VIII*; Oye, H., Ed.; NTNU: Trondheim, Norway, 2006; pp 235−238. (b) *Chem. Eng. News* **2008**, *86* (33), 16.
(3) *Ullmann's Encyclopedia of Industrial Chemistry*, 6th ed. (e-book); Wiley-VCH: Weinheim, Germany, 2002; Chapter: Silicon Compounds: Organic.
(4) (a) Campell-Ferguson, H. J.; Ebsworth, E. A. V. *J. Chem. Soc. A* **1966**, 1508–1514. (b) Campell-Ferguson, H. J.; Ebsworth, E. A. V. *J. Chem. Soc. A* **1967**, 705–712.
(5) Boudjouk, P.; Kloos, S. D.; Kim, B. K.; Page, M.; Thweatt, D. *J. Chem. Soc., Dalton Trans.* **1998**, 877–879.
(6) Wannagat, U.; Hensen, K.; Petesch, P. *Monatsh. Chem.* **1967**, *98*, 1407–1414.
(7) Fleischer, H.; Hensen, K.; Stumpf, T. *Chem. Ber.* **1996**, *129*, 765–771.

of the hexacoordinated compounds $HSiCl_3(Rpy)_2$,[9] which exhibit various substitution patterns (R) on the pyridine donor molecule (py). These solid adducts were found to be stable at room temperature (under inert atmosphere) and are directly accessible from trichlorosilane and the respective pyridine in various solvents.

Here we report high-yield syntheses of 2:1 pyridine adducts of $HSiCl_3$ and $HSiCl_2Me$, including a detailed spectroscopic and structural characterization. A comparison of the reactivities of the solid octahedral adducts shows that the methyl-substituted silane is stable against dismutation while trichlorosilane adducts tend to dismutate upon treatment with polar solvents and/or heat.

Experimental Section

The reactions were carried out under an inert atmosphere of dry argon using Schlenk techniques. Solvents were dried and purified by standard methods. The starting materials $HSiCl_3$ (Acros), $HSiCl_2Me$ (Aldrich), 4-methylpyridine (Alfa Aesar), 4-ethylpyridine (Merck), 3-bromopyridine (ABCR), 4-*tert*-butylpyridine (Fluka), 4-vinylpyridine (Aldrich), 4-phenylpyridine (Fluka), 4-dimethylaminopyridine (Fluka), and pyridine (Riedel de Haen) were commercially available. Liquid substituted and unsubstituted pyridines were heated over CaH_2 for several hours and then distilled and stored over 3 Å molecular sieve. Solid compounds were dried under vacuum for several hours. $HSiCl_3$ and $HSiCl_2Me$ were used as supplied. Cooled (0 °C) syringes were used for the addition of the required amounts of these silanes.

Cross-polarization/magic-angle spinning (CP/MAS) NMR spectra were recorded on a Bruker Avance 400 MHz WB spectrometer using a 7 mm probe head with zirconia rotors and Kel-F inserts operating at 400.23, 100.61, and 79.51 MHz for ^1H, ^{13}C, and ^{29}Si spectra, respectively. Chemical shifts are reported in parts per million relative to TMS. Raman spectra were recorded on a Bruker RFS 100/S instrument using a Nd:YAG laser.

Elemental analysis was performed on a CHN-O-Rapid analyzer. Determination of the chlorine content was performed by hydrolysis of 0.15 g of the corresponding silicon complex in 100 mL of diluted sodium hydroxide solution followed by chloride quantification using ion chromatography (Dionex ICS-2000, 22 mM KOH eluent, AS11_HC column, electrical conductivity measurement).

Single-crystal X-ray diffraction data were collected on a Bruker Nonius X8 APEX2 CCD diffractometer. Structures were solved with direct methods and refined with full-matrix least-squares methods. All non-hydrogen atoms were anisotropically refined. Carbon-bonded hydrogen atoms were placed in idealized positions and isotropically refined (riding model). Si-bonded hydrogen atoms were found by analysis of the residual electron density and refined without bond length restraints. Structure solution and refinement of F^2 against all reflections were carried out with SHELXS-97 and SHELXL-97 software (G. M. Sheldrick, Universität Göttingen, 1986−1997). Structure determination and refinement data for the crystal structures herein presented are summarized in Table S1 in the Supporting Information.

General Procedure for the Synthesis of 1a−h and 2. $HSiCl_3$ (5 mmol) was dissolved in toluene (20 mL), and the solution was stirred at −78 °C while the desired pyridine base (10 mmol) was added dropwise. Each product precipitated as a colorless solid. The suspension was stirred for 1 h at −78 °C and was then allowed to slowly adjust to ambient temperature. The white precipitate was filtered off, washed with toluene, and dried under vacuum. (Modifications to this procedure are outlined where applicable.) For the synthesis of compound **2**, no solvent was used. A Schlenk flask (at −78 °C) was charged with $HSiCl_3$ (5 mmol), after which 10 mmol of 2-methylpyrazine was added. For the syntheses of **3c** and **3g**, $HSiCl_3Me$ (5 mmol) was used instead of $HSiCl_3$. Further experimental details and additional analytical and spectroscopic data are provided in the Supporting Information.

Yields for Compounds 1a−h, 2, 3c, and 3g. Trichlorohydridobis(pyridine)silane (**1a**): 1.45 g (4.94 mmol; 98.8%). Trichlorohydridobis(3-bromopyridine)silane (**1b**): 1.26 g (2.79 mmol; 55.8%). Trichlorohydridobis(4-methylpyridine)silane (**1c**): 1.55 g (4.82 mmol; 96.3%). Trichlorohydridobis(4-ethylpyridine)silane (**1d**): 1.66 g (4.75 mmol; 95%). Trichlorohydridobis(4-vinylpyridine)silane (**1e**): 1.72 g (4.98 mmol; 99.5%). Trichlorohydridobis(4-*tert*-butylpyridine)silane (**1f**): 1.95 g (4.8 mmol; 96.1%). Trichlorohydridobis(4-dimethylaminopyridine)silane (**1g**): 1.85 g (4.87 mmol; 97.4%). Trichlorohydridobis(4-phenylpyridine)silane (**1h**): 2.21 g (4.95 mmol; 99%). Trichlorohydridobis(2-methylpyrazine)silane (**2**): 1.60 g (4.94 mmol; 98.9%). Methyldichlorohydridobis(4-methylpyridine)silane (**3c**): 1.44 g (4.85 mmol; 97%). Methyldichlorohydridobis(4-dimethylaminopyridine)silane (**3g**): 1.74 g (4.9 mmol; 98%).

Quantum-Chemical Calculations. The quantum-chemical calculations were carried out using the Gaussian03 series of programs.[10] NMR shielding tensors were calculated with the gauge-independent atomic orbital (GIAO) method[11] using the B3LYP density functionals[12,13] in combination with the 6-311+G(2d,p) basis set for all atoms[14−16] at the geometries from the X-ray structure analyses. Calculated absolute shielding values were converted to chemical shifts (δ) relative to the shielding for tetramethylsilane calculated at the same level of theory. The molecular geometries of **1c** and **3c** were optimized at the B3PW91/6-31G(d,p) level.[15−17] Previous investigations have shown that this method/basis-set combination gives the best agreement of the optimized geometry with the geometry obtained from X-ray structure analysis for more highly coordinated silicon complexes.[18] The quantum theory of atoms in molecules (QTAIM) analyses[30] were performed at the B3PW91/6-31G(d,p) level with the optimized geometries. The wave function files for the QTAIM analyses were generated in Cartesian coordinates with a basis set containing 6d functions (option "6D 10F" in Gaussian03). The electron density topology was analyzed using the programs AIM2000[19] and Xaim.[20] The natural charges were obtained from calculations with NBO 5.0.[21]

Results and Discussion

Compounds **1a−h** and **2** (Scheme 1) were synthesized in an aprotic solvent such as *n*-hexane, toluene, or THF. In analogy to the previously described direct reaction of H_2SiCl_2 with pyridines, the initial formation of the octahedrally coordinated silicon compounds $HSiCl_3(Rpy)_2$ was to be expected.[8]

(8) Fester, G. W; Wagler, J.; Brendler, E.; Böhme, U.; Roewer, G.; Kroke, E. *Chem.−Eur. J.* **2008**, *14*, 3164–3176.
(9) Fester, G. W.; Wagler, J.; Brendler, E.; Kroke, E. *Eur. J. Inorg. Chem.* **2008**, 5020–5023.
(10) Frisch, M. J.; et al. *Gaussian 03*, revision C.02; Gaussian, Inc.: Wallingford, CT, 2004.
(11) Wolinski, K.; Hinton, J. F.; Pulay, P. *J. Am. Chem. Soc.* **1990**, *112*, 8251–8260.
(12) Becke, A. D. *J. Chem. Phys.* **1993**, *98*, 5648–5652.
(13) Stevens, P. J.; Devlin, F. J.; Chablowski, C. F.; Frisch, M. J. *J. Phys. Chem.* **1994**, *98*, 11623–11627.
(14) Hehre, W. J.; Radom, L.; Schleyer, P. v. R.; Pople, J. A. *Ab Initio Molecular Orbital Theory*; Wiley: Chichester, U.K., 1986.
(15) Hariharan, P. C.; Pople, J. A. *Theor. Chim. Acta* **1973**, *28*, 213–222.
(16) Francl, M. M.; Pietro, W. J.; Hehre, W. J.; Binkley, J. S.; Gordon, M. S.; DeFrees, D. J.; Pople, J. A. *J. Chem. Phys.* **1982**, *77*, 3654–3665.
(17) Perdew, J. P.; Burke, K.; Wang, Y. *Phys. Rev. B* **1996**, *54*, 16533–16539.
(18) Fels, S. Diploma Thesis, TU Bergakademie Freiberg, Freiberg, Germany, 2007.
(19) Biegler-König, F.; Schönbohm, J.; Bayles, D. *J. Comput. Chem.* **2001**, *22*, 545–559.
(20) Ortiz, J. C.; Bo, C. *Xaim*; Universitat Rovira i Virgili, Tarragona, Spain.
(21) Glendening, E. D.; Badenhoop, J. K.; Reed, A. E.; Carpenter, J. E.; Bohmann, J. A.; Morales, C. M.; Weinhold, F. *NBO 5.0*; Theoretical Chemistry Institute, University of Wisconsin: Madison, WI, 2001.

Scheme 1. Reaction of Trichlorosilane with Substituted Pyridines

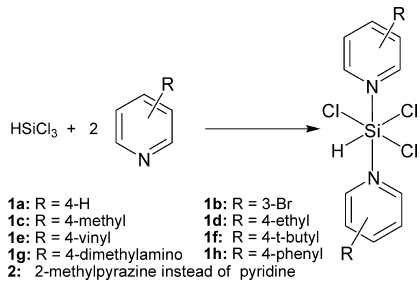

The hexacoordinated silicon complexes were characterized by ^{13}C and ^{29}Si CP/MAS NMR as well as Raman spectroscopy and, when possible, by single-crystal X-ray diffraction. The poor solubilities of the complexes rendered solution NMR spectroscopy unsuitable. Products **1a**−**c**, **1g**, **1f**, and **3g** were additionally characterized by elemental analyses.

As expected, the Si−H valence vibration band in the Raman spectrum was shifted to lower wavenumbers compared with the corresponding band in $HSiCl_3$, and this was accompanied by broadening of the signal. Compounds **1a**−**h** and **2** exhibited a characteristic Si−H valence vibration band at 2061−2128 cm^{-1} (see Table 1). The latter observation can be attributed to increasing ionic contributions to the Si−H bonds. The ^{29}Si NMR shifts (δ_{iso}) ranged between −164.8 and −172.0 ppm, confirming hexacoordination of the silicon atom.[22] In comparison with those of the previously reported dichlorosilane adducts $H_2SiCl_2(Rpy)_2$, the resonances of all the $HSiCl_3(Rpy)_2$ compounds were significantly shifted to higher field (by ∼20 ppm). This effect can be attributed to the substitution of one Si-bound hydrogen atom by a Cl substituent.

With increasing electron-releasing effects of the substituents at the pyridine moiety, the Si atoms gain electron density, leading to a high-field shift of the ^{29}Si NMR signal. This is most obvious for **1g** because of the strong mesomeric effect of the dimethylamino substituent.[5]

As pointed out in the Introduction, most intermolecular hypercoordinated Lewis base adducts of chlorosilanes are stable only in the solid state (they dissociate upon dissolution or melting). A simple method to investigate the stability of $HSiCl_3(Rpy)_2$ compounds relative to each other is the use of exchange reactions with pyridines having different substituents.

The observed exchange of the pyridine ligands in the complex $HSiCl_3(py)_2$ with 4-dimethylaminopyridine (4-DMAP) (eq 2) suggests that **1g** is more stable than **1a**. Notably, this ligand exchange proceeds in THF at 20 °C without significant H-versus-Cl dismutation.

$$HSiCl_3(py)_2 + 2(4\text{-DMAP}) \rightarrow HSiCl_3(4\text{-DMAP})_2 + 2py \quad (2)$$

Under the synthesis conditions applied here (−78 °C), the trichlorosilane pyridine adducts precipitated immediately. In order to obtain single crystals suitable for X-ray diffraction analyses, recrystallization from various solvents was attempted. Despite the lack of stability of the above complexes in solution, we succeeded in crystallizing three compounds (**1b**,[8] **1f**, and **1h**). Their molecular structures are depicted in Figure 1.

Unlike the dichlorosilane adducts $H_2SiCl_2(Rpy)_2$, all of which exhibited the Si atom on a crystallographically imposed center of symmetry,[7] only **1h** bears half a molecule in the asymmetric unit. The Si atom of **1h** is located on a center of inversion, thus generating the second 4-phenylpyridine ligand. The location on this symmetry element results in a 1:1 disorder of the Si-bound hydrogen atom and the trans-situated chlorine atom Cl2 (for clarity, only one arrangement is depicted in Figure 1). Compounds **1b** and **1f** exhibit one Si complex per asymmetric unit, and the Si−H bond is not influenced by any symmetry-imposed effects of disorder. However, compound **1b** crystallized with half a molecule of 3-bromopyridine in the asymmetric unit, which is located near a center of inversion and is therefore part of a symmetry-imposed disorder.

The Si−N distances, which range between 197.5(3) and 198.9(3) pm, are slightly longer than in the previously reported dichlorosilane adducts.[7] This slight Si−N bond lengthening is expected to be a result of the increased steric impact around the Si atom. Whereas in the dichlorosilane adducts the pyridine planes are tilted away from the Cl−Si−Cl axis by ∼70−80° and the Si−H bonds are nearly in plane with the pyridine ligands, the third Si-bound chlorine atom forces the other two Cl atoms closer to the pyridine 2,6-hydrogen atoms. The Si−Cl bonds of the above trichlorosilane adducts fall in the ranges 218.3(1)−223.7(1) pm for Cl2 and 221.9(1)−226.3(1) pm for the other two Si−Cl bonds and are thus significantly shorter than those in the dichlorosilane complexes. This Si−Cl bond shortening is well in accord with the Si−N bond lengthening.

The shorter Si−Cl bonds support the following observation: contrary to the experiments described for dichlorosilane (where formation of $[H_2Si(Rpy)_4]^{2+}$ complexes was possible), cationic species of the type $[HClSi(Rpy)_4]^{2+}$ have not been observed to date.[23] Both the increased steric demand around the Si atom and the stronger (shorter) Si−Cl bonds (versus the longer Si−N bonds) render the addition of two additional pyridine molecules less likely. Furthermore, the dissociation of the Si−X bonds depends on a variety of parameters, in particular, temperature, solvent, the nature of the anion, and further substituents on the Si atom.[24,25] Whereas alkyl groups promote the formation of more highly coordinated siliconium cations, electron-withdrawing substituents (e.g., additional chlorine atoms) inhibit ionic Si−Cl dissociation.

The predominant decomposition reaction observed for the $HSiCl_3$ adducts was H-versus-Cl redistribution. This dismutation yields pyridine adducts of $SiCl_4$ and H_2SiCl_2 that are formed upon treatment with polar solvents at elevated temperatures. Thus, mixtures of complexes of $SiCl_4$, $HSiCl_3$, and H_2SiCl_2 with the respective substituted pyridines were obtained (Scheme 2).

Among the pyridine adducts under investigation, compounds **1f** and **1h** exhibited the lowest tendency for dismutation. This observation could not be explained by increased or decreased donor properties of the pyridines. Hence, effects such as lower solubilities may account for their increased stabilities.

The dismutation reactions were monitored by ^{29}Si CP/MAS NMR spectroscopy. Whereas the complexes synthesized at lower temperatures delivered spectra with only one signal, indicative of the $HSiCl_3(Rpy)_2$ complex (Figure 2), prolonged heating in polar solvents delivered solids that exhibited signals of the dichlorosilane complex $H_2SiCl_2(Rpy)_2$ and an additional

(22) Kintzinger, J. P.; Marsmann, C. *NMR: Basic Principles and Progress, Vol 17*; Springer: Berlin, 1981.

(23) Hensen, K.; Kettner, M.; Stumpf, T.; Bolte, M. *Z. Naturforsch., B* **2000**, *55*, 901–906.

(24) Gostevskii, B.; Silbert, G.; Adear, K.; Sivaramakrishna, A.; Stalke, D.; Deuerlein, S.; Kocher, N.; Voronkov, M.; Kalikhman, I.; Kost, D. *Organometallics* **2005**, *24*, 2913–2920.

(25) Kost, D.; Kingston, V.; Gostevskii, B.; Ellern, A.; Stalke, D.; Walfort, B.; Kalikhman, I. *Organometallics* **2002**, *21*, 2293–2305.

Table 1. ^{29}Si CP/MAS NMR Data, Selected Bond Lengths, and ν(Si−H) Raman Bands for Compounds **1a**−**h**, **2**, **3c**, **3g**, $HSiCl_3$, and $MeHSiCl_2$ (Compounds Are Ordered According to Their ^{29}Si NMR Shifts)

	R	δ_{iso} ^{29}Si (ppm)	d(Si−N) (pm)	d(Si−Cl2) (pm)	d(Si−Cl1) (pm)	ν(Si−H) (cm^{-1})
$HSiCl_3$		−9.6[a]		202.0(3)[b]	202.0(3)[b]	2244[c]
1a	H	−164.8				2095
1c	4-CH_3	−165.0				2077
1h	4-C_6H_5	−165.6	197.8(2)	223.7(1)	226.3(1)	2092
1b	3-Br	−165.7	198.2(3), 198.9(3)	218.3(1)	221.9(1) 222.7(1)	2093
1e	4-$CHCH_2$	−168.2				2111
1d	4-CH_2CH_3	−168.5				2092
2		−168.9				2089
1f	4-$C(CH_3)_3$	−170.0	197.5(3),198.0(3)	218.6(1)	222.7(1) 223.3(1)	2128
1g	4-$N(CH_3)_2$	−172.0				2061
$MeHSiCl_2$		10.3		204.0[d]	204.0[d]	2218
3c	4-CH_3	−135.6	199.8(1), 202.0(1)	235.6(1)	227.0(1)	2092
3g	4-$N(CH_3)_2$	−141.3	198.0(1), 198.5(1)	236.8(1)	227.7(1)	2058

[a] Data from ref 41. [b] Data from refs 42 and 43. [c] Data from ref 44. [d] Data from ref 45.

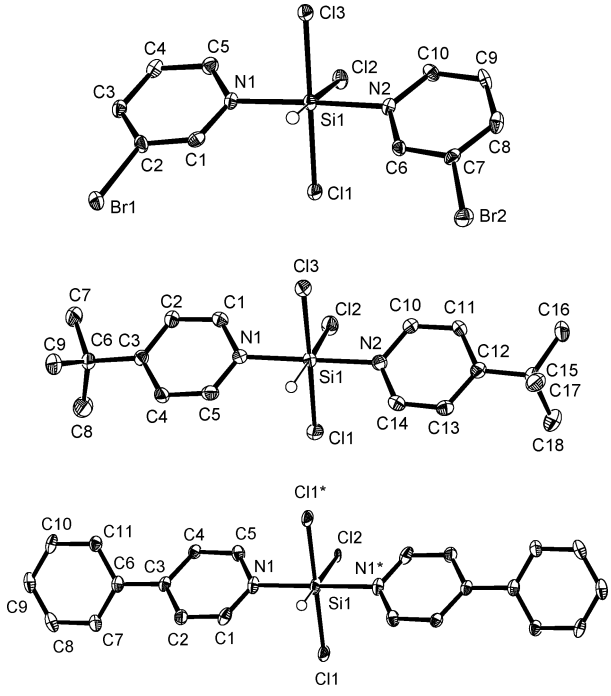

Figure 1. Molecular structures of (top) **1b**, (middle) **1f**, and (bottom) **1h**, shown as ORTEP diagrams with thermal ellipsoids at the 50% probability level. C-bound hydrogen atoms have been omitted, and selected atoms are labeled.

Scheme 2. Dismutation of $HSiCl_3(Rpy)_2$ in Polar Solvents at Elevated Temperatures

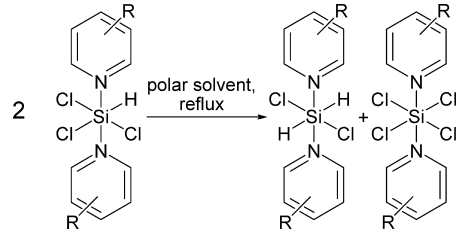

signal at higher field that can be attributed to the complex $SiCl_4(Rpy)_2$. Although several silicon tetrachloride adducts have been reported,[26] for unambiguous assignment of the latter signals, selected $SiCl_4(Rpy)_2$ complexes were synthesized from $SiCl_4$ and characterized by solid-state ^{29}Si NMR spectroscopy. Unfortunately, the $H_2SiCl_2(Rpy)_2$ complex continued to dismutate under the applied conditions to form H_3SiCl, SiH_4, and $SiCl_4(Rpy)_2$. This is the reason for the missing signal in the

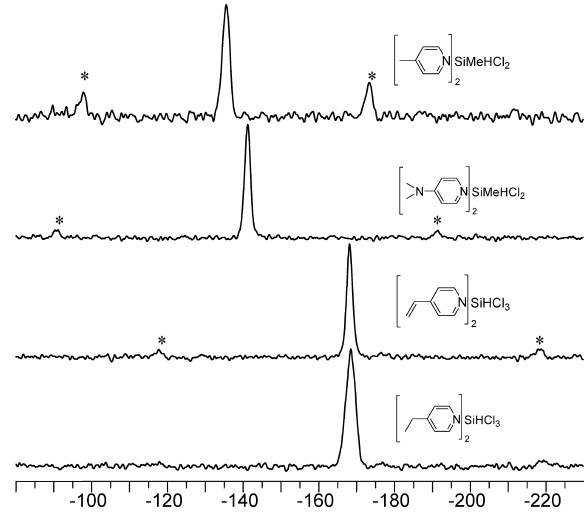

Figure 2. ^{29}Si CP/MAS NMR spectra of (from top to bottom) **3c**, **3g**, **1e**, and **1d**. Asterisks mark spinning sidebands.

^{29}Si CP/MAS NMR spectrum. Only small quantities of trichlorosilane−pyridine adducts remained (Figures 2 and 3).

Time-dependent ^{29}Si NMR investigations of the solids during the course of the dismutation process indicated that the $SiCl_4$ adducts are less soluble than the H_2SiCl_2 adducts. Similar observations were made upon recrystallization of the products.

The dismutation reactions were prevented by substituting one Si-bound Cl atom in $HSiCl_3$ with a methyl group. For example, the methyldichlorosilane adducts **3c** and **3g** were prepared in good yield (Scheme 3). Their molecular structures were determined by X-ray diffraction analysis (Figure 4). Surprisingly, none of the other adducts of $HSiCl_2Me$ and the substituted pyridines investigated in the present study were stable at room temperature. Syntheses at room temperature without solvent delivered unstable products. This was indicated by NMR and Raman spectroscopy of the corresponding reaction products. ^{29}Si NMR spectra of solutions of **3c** and **3g** exhibited signals for $HSiCl_2Me$ and the respective pyridines only.

The decreased Lewis acidity of the Si atom (with respect to trichlorosilane) accounts for the following observations: The

(26) For example, see: (a) Denmark, S. E.; Eklov, B. M. *Chem.—Eur. J.* **2008**, *14*, 234–239. (b) Hensen, K.; Mayr-Stein, R.; Spangenberg, B.; Bolte, M.; Ruhl, S. *Z. Naturforsch., B* **2000**, *55*, 248–252. (c) Jalil, N. S. N.; Oluwabunmi, A. V. *Phosphorus, Sulfur Silicon Relat. Elem.* **1996**, *119*, 151–159. (d) Bechstein, O.; Ziemer, B.; Hass, D.; Troyanov, S. I.; Rybakov, V. B.; Maso, G. N. *Z. Anorg. Allg. Chem.* **1990**, *582*, 211–216.

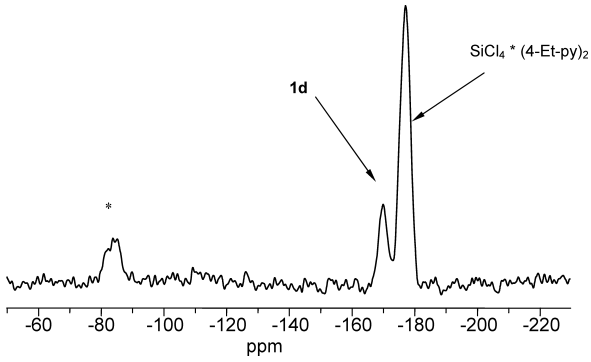

Figure 3. ^{29}Si CP/MAS spectrum of the product obtained by dismutation of **1d** in acetonitrile under reflux for 6 h. The asterisk marks a signal from the decomposition product.

Scheme 3. Reaction of Methyldichlorosilane with Substituted Pyridines

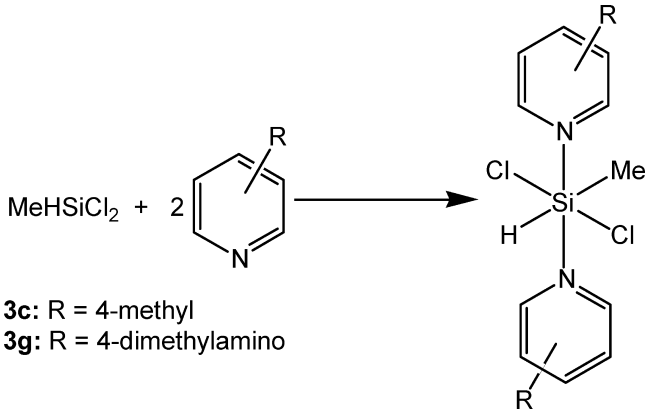

methyldichlorosilane adducts exhibit noticeably longer Si−N distances [198.0(1) and 198.5(1) pm for **3g**; 199.8(1) and 202(1) pm for **3c**] and Si−Cl distances [227.7(1) and 227.0(1) pm for Cl1 in **3g** and **3c**, respectively; 236.8(1) and 235.6(1) pm for Cl2 in **3g** and **3c**, respectively]. The pyridine ligands are slightly bent toward chlorine atom Cl2 [the N−Si−N angles are 172.6(1)° and 173.7(1)° for **3c** and **3g**, respectively], showing the longer Si−Cl distance and hinting at the previously mentioned trend of alkyl-supported ionic Si−Cl dissociation. As noted for the $HSiCl_3$ complexes, 4-DMAP exerts a stronger donor activity, which results in a pronounced Si−N bond shortening and Si−Cl bond lengthening in **3g** compared with **3c**. Contrary to the ionic polarization in the solid state, the methyldichlorosilane adducts dissociated quantitatively in solution to yield the starting materials; this fact supports the stability of $HSiCl_2Me$ toward dismutation reactions. This dissociation, however, cannot be the only key to the increased stability, as shown in the following example: Sterically hindered pyridines [e.g., 2,6-disubstituted pyridines such as 2,6-dimethylpyridine (lutidine) and 2,4,6-trimethylpyridine (collidine)] did not form isolable octahedral silicon complexes $HSiCl_3(Rpy)_2$. However, this kind of substituted pyridine base still supports the dismutation of trichlorosilane (eq 3):

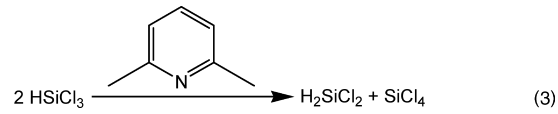

(3)

The steric demand of the substituents may be responsible for this lack of capability to form hexacoordinated trichlorosilane

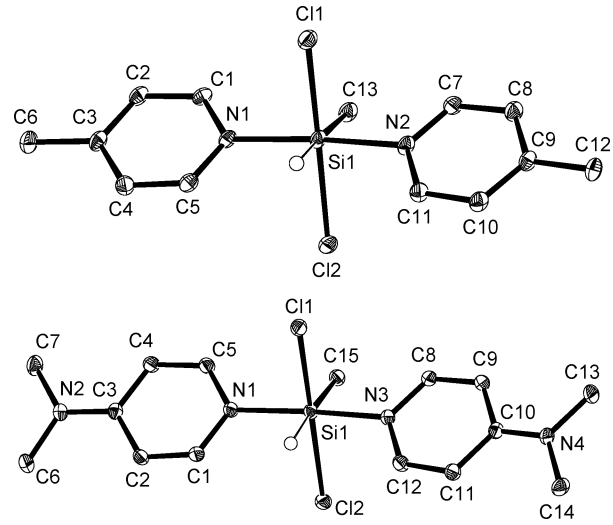

Figure 4. Molecular structures of (top) **3c** and (bottom) **3g**, shown as ORTEP diagrams with thermal ellipsoids at the 50% probability level. C-bound hydrogen atoms have been omitted, and non-hydrogen atoms are labeled.

complexes. In addition to the decreased Lewis acidity (with respect to $HSiCl_3$), methyldichlorosilane has a lower Brønsted acidity, which could explain the inhibition of the H-versus-Cl dismutation reaction. The 2,6-disubstituted pyridines are still bases capable of deprotonating trichlorosilane. Such deprotonation might, in addition to Si hypercoordination, represent another key step in the H-versus-Cl dismutation observed for trichlorosilane.

The ^{29}Si solid-state NMR characterization of the trichlorosilane adducts reported herein gave rise to the observation that the octahedral complexes $HSiCl_3(Rpy)_2$ exhibit noticeably less anisotropic signals than their dichlorosilane analogues $H_2SiCl_2(Rpy)_2$.[5,8] To elucidate the origin of this observation, the ^{29}Si chemical-shift tensors of compounds **1b**, **1h**, **1f**, **3c**, and **3g** were calculated on the basis of the solid-state geometry. This guaranteed the best consistency with the experimentally determined solid-state NMR data.

Comparison of the experimental and calculated values shows very good agreement for the isotropic shift and span for the $HSiCl_3$ compounds. Differences can be observed for the principal components and therefore the span, where the observed values are larger than the calculated ones. There is very good agreement for δ_{22}, but significant differences exist for δ_{33}. The largest deviations are found for δ_{11} corresponding to the direction of lowest shielding, which is perpendicular to the Si−H bond. The same effect has been observed for the H_2SiCl_2 adducts and can probably be attributed to inherent problems with the calculations on compounds containing Si−H bonds.[5,27,28] In addition, inaccuracies in the experimental results must be taken into account because of residual dipolar couplings between silicon and the three chlorine atoms, which may not be completely averaged at the low spinning rates used to generate the spinning-sideband spectra for the tensor measurements.

Analysis of the ^{29}Si NMR tensor components with the GIAO method allows assignment of the tensor components in the coordinate system of the molecule. Three different orientations

(27) Corminboeuf, C.; Heine, T.; Weber, J. *Chem. Phys. Lett.* **2002**, *357*, 1–7.
(28) Heine, T.; Goursot, A.; Seifert, G.; Weber, J. *J. Phys. Chem. A* **2001**, *105*, 620–626.

Table 2. ^{29}Si MAS NMR Data and Results of GIAO Calculations [B3LYP/6-311+G(2d,p)] of ^{29}Si NMR Shifts of Compounds **1** and **3**

	R		δ_{iso}[a]	δ_{11}	δ_{22}	δ_{33}	Ω[b]	κ[b]
				$HSiCl_3$				
1h	4-C_6H_5	calcd	−164.8	−131.4	−181.0	−182.1	50.7	−1.0
		exptl	−165.6	−110.7	−182.2	−203.9	93.2	−0.54
1b	3-Br	calcd	−162.2	−122.6	−177.5	−186.6	64.0	−0.7
		exptl	−165.7					
1f	4-$C(CH_3)_3$	calcd	−171.5	−141.7	−181.4	−191.4	49.7	−0.6
		exptl	−170.0	−126.6	−183.3	−202	75.5	−0.45
				$MeHSiCl_2$				
3c	4-CH_3	calcd	−150.9	−99.9	−163.9	−188.9	89.0	−0.4
		exptl	−135.7	−74.8	−145.7	−186.6	111.9	−0.27
3g	4-$N(CH_3)_2$	calcd	−157.4	−120.1	−160.7	−191.2	71.1	−0.1
		exptl	−141.3	−98.7	−142.3	−182.4	83.7	−0.04

[a] Chemical shift in the solid state. [b] In the Herzfeld−Berger convention,[46] $\Omega = \delta_{11} - \delta_{33}$ and $\kappa = 3(\delta_{22} - \delta_{iso})/\Omega$.

of the ^{29}Si NMR tensor components were found for the compounds under investigation (see Table 2 and Figure 5). In nearly all of the compounds, the principal axes are oriented along the main bond axes. The higher shielding of the silicon atoms in **1b** and **1f** is along the N−Si−N and H−Si−Cl axes (δ_{33} and δ_{22}, respectively). Noticeably lower shielding is observed along the Cl−Si−Cl axis (δ_{11}). In compound **1h**, the lowest shielding is also oriented along the Cl−Si−Cl axis. Surprisingly, the two higher-shielding tensor components (δ_{33} and δ_{22}) bisect the H−Si−N and Cl2−Si−N bond angles, respectively. This can be explained by the nearly identically values of δ_{33} and δ_{22}, which generate a circular plane of equal shielding that includes the N−Si−N and H−Si−Cl axes. Another orientation of tensor components was observed for the $HSiCl_2Me$ adducts **3c** and **3g**. The lowest shielding (δ_{11}) is again along the Cl−Si−Cl axis. As an effect of the methyl group, the highest shielding (δ_{33}) is now along the H−Si−Me axis. Comparison of the principal components of the compounds shows that the changes in δ_{iso} and Ω are mainly due to changes in δ_{11}, which is perpendicular to the Si−C (vs the Si−Cl) bond and the longer (vs the shorter) Si−Cl bonds, whereas δ_{22} is very similar and δ_{33} shows only minor variations. This finding is in agreement with a previous report, which underlines the fact that a principal component of the ^{29}Si NMR shielding is mainly influenced by the substituents perpendicular to its direction.[29]

Quantum-chemical calculations were performed in order to obtain insight into the distinct features of the bonds between silicon and the surrounding ligands in these types of octahedral complexes. The compounds **1c** and **3c** were chosen as representative derivatives. The topology of the electron density distribution was investigated using QTAIM analysis, as developed by Bader and others.[30−34] This method partitions the electron density of a molecule, $\rho(\mathbf{r})$, into individual nonoverlapping atomic fragments through the use of rigorously defined interatomic surfaces. Various properties can be derived from the electron density distribution. The electron density in a molecule is a three-dimensional function that has four types of extrema: maxima, minima, and two types of saddle points. The maxima coincide with the nuclear positions. Minima are found in the center of cage molecules and are called cage critical points. Saddle points that are a maximum in one dimension and a minimum in two dimensions are called ring critical points (RCPs). These are found in the center of atomic rings. Saddle points that are a maximum in two dimensions and a minimum in one dimension are called bond critical points (BCPs). When a BCP is found between two atoms, an atomic interaction line can be drawn. When the molecule is in its equilibrium geometry, the atomic interaction line is called a bond path. A bond path is not identical with a bond in the sense used by a Lewis structure. Bond paths are observed for predominately ionic bonds, covalent bonds, weak hydrogen bonds, and even interactions between anions. The Laplacian of the electron density ($\nabla^2\rho$) at the BCP between two atoms gives essential information about the nature of the bond between the involved atoms. The second partial derivatives of the charge density with respect to the coordinates are expressed as the Hessian matrix, diagonalization of which yields the principal curvatures (eigenvalues) $\lambda_1 < \lambda_2 < \lambda_3$. The ellipticity of a bond is defined as $\varepsilon = (\lambda_1/\lambda_3) - 1$. The algebraic sum of the three principal curvatures λ_1, λ_2, and λ_3 is equal to $\nabla^2\rho$ at the BCP. The nature of the atomic

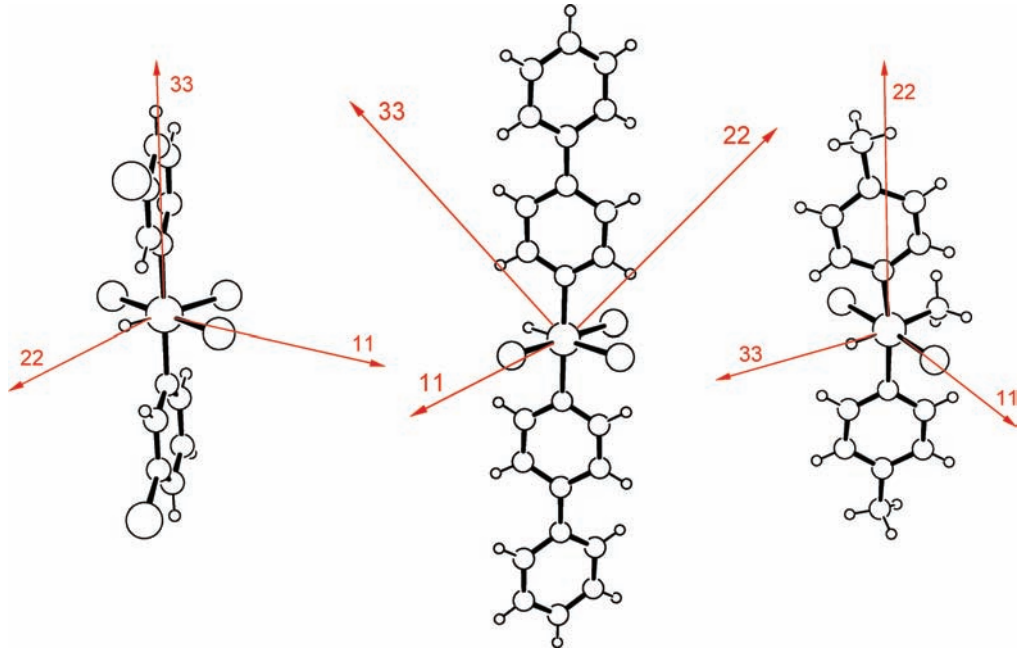

Figure 5. Orientations of the principal shielding tensor components in (left) **1b** and **1f**, (middle) **1h**, and (right) **3c** and **3g**.

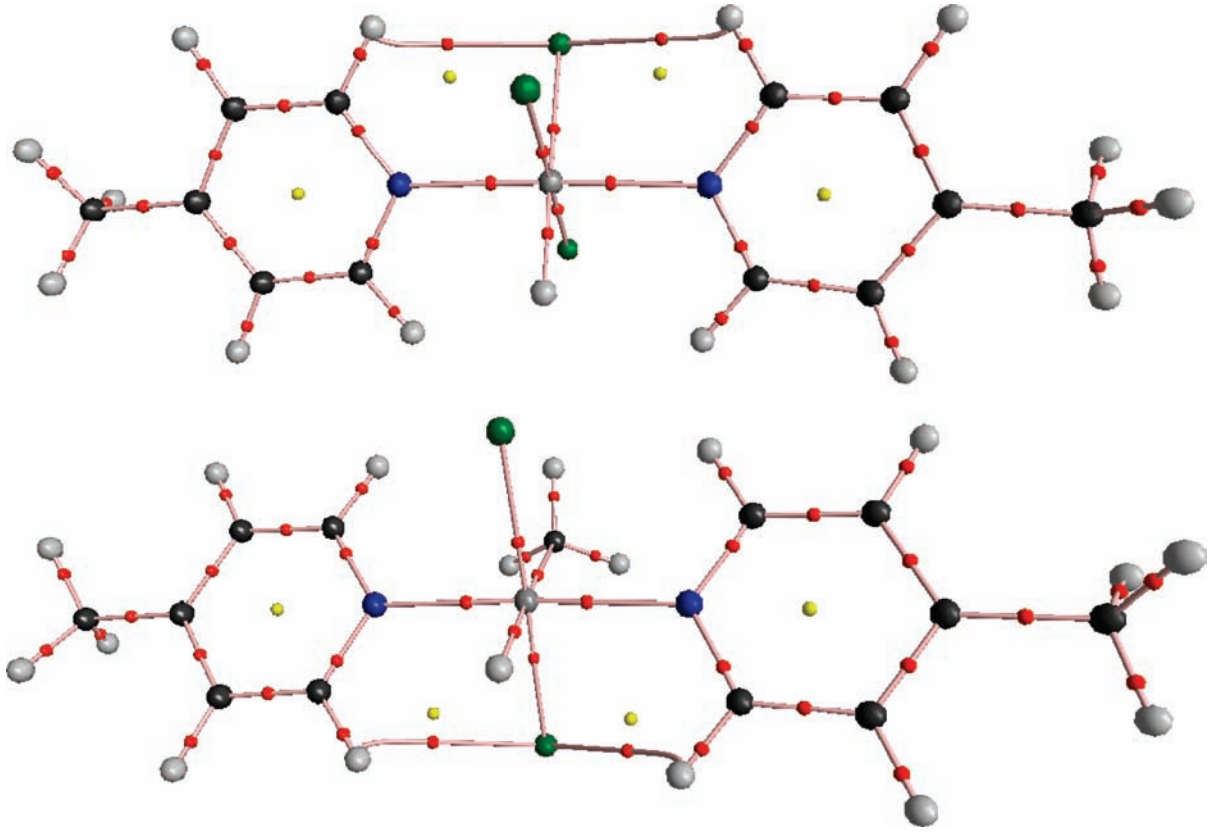

Figure 6. Molecular graphs of (top) **1c** and (bottom) **3c**. Critical points are shown (BCPs in red, RCPs in yellow), and atomic spheres are drawn with arbitrary radii.

interactions depends on the dominant curvatures.[35] Covalent bonds (shared interactions) are dominated by the negative curvatures λ_1 and λ_2, which means that charge is concentrated in the internuclear region. The charge concentration leads to a large value of $\rho(\mathbf{r})$ and a negative value of the Laplacian $\nabla^2\rho$. For ionic interactions (closed-shell interactions), the positive curvature λ_3 is dominant, and charge is depleted at the BCP. The electron density is concentrated at the negatively charged atom, and the spatial distribution of the Laplacian is predominately atom-like (i.e., a spherical distribution). The charge depletion at the BCP leads to a small value of $\rho(\mathbf{r})$ and a positive value of $\nabla^2\rho$. A wide range of bonding situations intermediate between these two extremes are possible and have been discussed in the literature.[32,36]

The molecular graphs of the two molecules are shown in Figure 6. With one exception, the BCPs between the atoms in these molecules have the expected topology that one would describe with a classical Lewis structure. A surprising feature of both graphs is the presence of BCPs between two α-hydrogen atoms of the pyridine rings and one chlorine atom. According to the topological features of these unexpected BCPs, namely, ~1 order of magnitude smaller electron density than for the other BCPs (see Table 3) and a positive value for $\nabla^2\rho$,[34] both interactions can be classified as C−H···Cl contacts. These intramolecular contacts generate two −Si−N−C−H···Cl− rings in the molecule whose RCPs are located close to the BCPs of the corresponding contacts.

Table 3. Electron Density ρ (e/Å^3), Its Laplacian $\nabla^2\rho$ (e/Å^5), and Bond Ellipticity ε at Selected BCPs in **1c** and **3c**

		1c	3c
Si−Cl[a]	ρ	0.494[c]	0.443
	$\nabla^2\rho$	1.313[c]	1.007
	ε	0.200[c]	0.336
Si−Cl[b]	ρ	0.549	0.416
	$\nabla^2\rho$	1.891	0.547
	ε	0.074	0.503
Si−N	ρ	0.477	0.424
	$\nabla^2\rho$	4.266	3.316
	ε	0.102	0.325
Si−H	ρ	0.826	0.827
	$\nabla^2\rho$	5.151	5.126
	ε	0.044	0.040
Si−C	ρ		0.788
	$\nabla^2\rho$		5.105
	ε		0.037
H···Cl	ρ	0.084	0.074
	$\nabla^2\rho$	1.176	1.026
	ε	0.445	0.584

[a] Chlorine without hydrogen contacts. [b] Chlorine with hydrogen contacts. [c] Average values.

Contour maps of the electron density distribution and the Laplacian of the electron density are shown for **1c** and **3c** in Figures 7 and 8, respectively. The values of ρ and $\nabla^2\rho$ for the

(29) Gerlach, D.; Brendler, E.; Heine, T.; Wagler, J. *Organometallics* **2007**, *26*, 234–240.
(30) Bader, R. F. W. *Atoms in Molecules: A Quantum Theory*; Clarendon Press: Oxford, U.K., 1994.
(31) Gillespie, R. J. *J. Chem. Educ.* **2001**, *78*, 1688–1690.
(32) Gillespie, R. J.; Popelier, P. L. A. *Chemical Bonding and Molecular Geometry*; Oxford University Press: New York, 2001.
(33) Bader, R. F. W.; Essén, H. *J. Chem. Phys.* **1984**, *80*, 1943–1960.
(34) Koch, U.; Popelier, P. L. A. *J. Phys. Chem.* **1995**, *99*, 9747–9754.
(35) Kocher, N.; Selinka, C.; Leusser, D.; Kost, D.; Kalikhman, I.; Stalke, D. *Z. Anorg. Allg. Chem.* **2004**, *630*, 1777–1793.
(36) *The Quantum Theory of Atoms in Molecules*; Matta, C. F., Boyd, R. J., Eds.; Wiley-VCH: Weinheim, Germany, 2007.

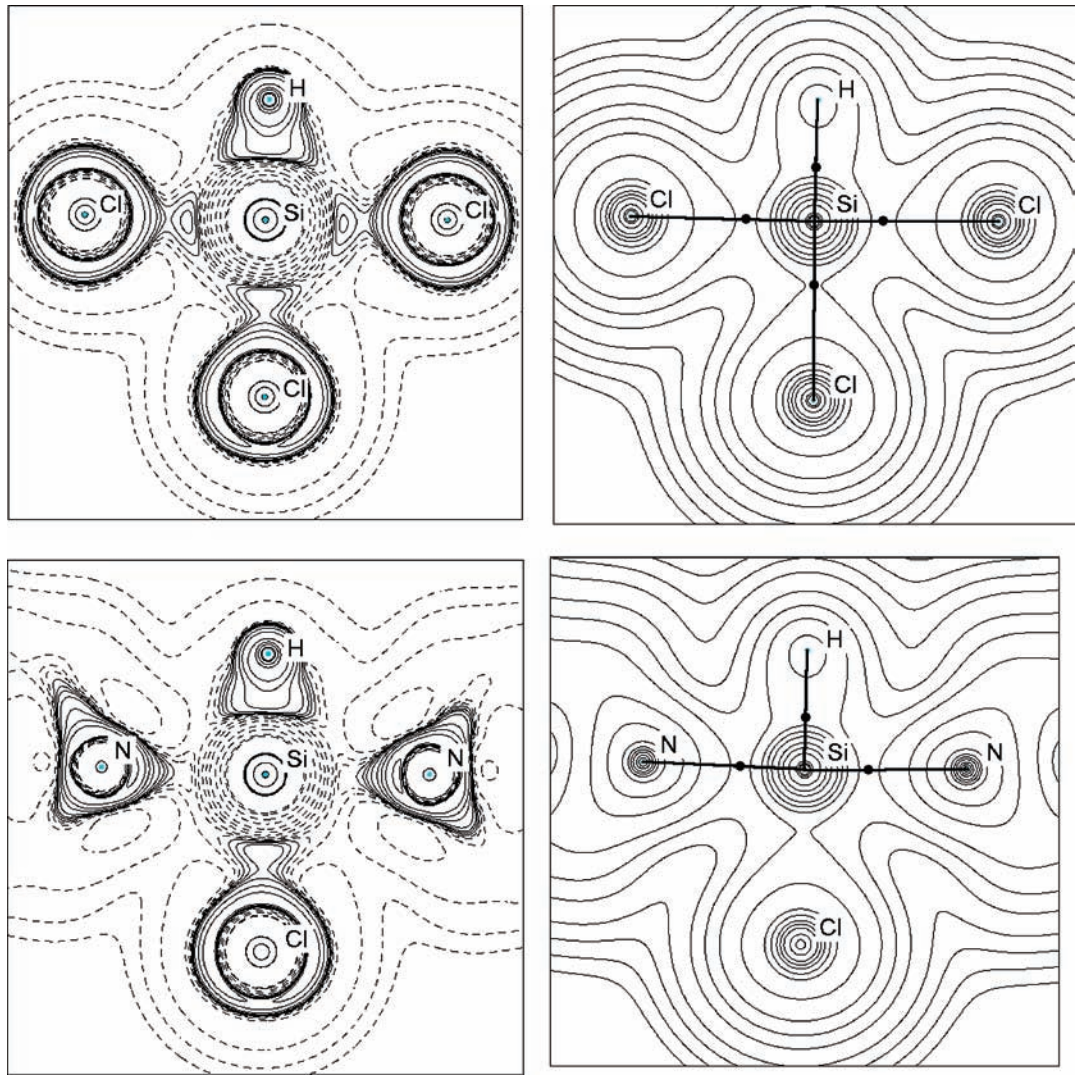

Figure 7. Representations of topological properties of **1c** in different planes: (top) $HSiCl_3$; (bottom) $HSiN_2$. It should be noted that the chlorine atom at the bottom of the $HSiCl_3$ graphics lies outside this plane. (left) Laplacian of the electron density. Positive values of $\nabla^2\rho$ are drawn with dashed lines and represent regions of charge depletion; negative values of $\nabla^2\rho$ are drawn with solid lines and represent regions of charge concentration. (right) Electron density. Selected bond paths and BCPs are drawn on the figures. The contour values for both representations in atomic units are 0.001, 0.002, 0.004, 0.008, 0.02, 0.04, 0.08, 0.2, 0.4, 0.8, 2, 4, 8, 20, 40, 80, 200, 400, and 800.

BCPs between silicon and the six surrounding atoms are summarized in Table 3. The properties of the electron density distribution at these BCPs allow conclusions to be drawn about the bond features. The interactions between Si and Cl are mainly ionic, as can be seen in the graphical representation of $\nabla^2\rho$ (Figure 7, left), where there is a nearly spherical accumulation of electron density around each chlorine atom. The electron density at the BCP between Si and Cl is in the range 0.4−0.5 e/Å^3. The positive values of $\nabla^2\rho$ also hint at a closed-shell interaction. The BCP between Si and the Cl trans to H in **1c** has the largest value of ρ (0.549 e/Å^3) among all of the chlorine atoms in both molecules, indicating that more electron density is accumulated in the interatomic space between these two atoms than around any other BCP between Si and Cl. This effect can be attributed to the electron-donating character of the hydrogen atom located trans to this bond. The interactions between Si and N are also mainly ionic. This is visualized in the representation of $\nabla^2\rho$, where the interatomic space between Si and N is depleted of electron density. The electron densities at the BCPs between Si and N have values similar to those for the Si−Cl interactions, but $\nabla^2\rho$ is 3- to 6-fold higher. The lone pairs on nitrogen, which are responsible for the donor−acceptor interactions, can be seen as small areas of charge concentration localized on the nitrogen atoms and directed toward silicon in the graphical representations of $\nabla^2\rho$ (Figures 7 and 8, lower left). Slightly pronounced bond ellipticities at the Si−N and Si−Cl BCPs hint at the presence of additional π donation from the lone pairs on chlorine and the aromatic system of the pyridine rings. The charge density of the hydrogen atom is polarized toward the positively charged silicon atom (Figures 7 and 8), which leads to a notable charge concentration along the Si−H bond axis and a larger electron density at the BCPs. This can be interpreted as a polar covalent bond. The positive value of the Laplacian disagrees with a covalent character. A closer examination of the position of the BCP in this case shows that the BCP is located close to the nodal surface in $\nabla^2\rho$, on each side of which the atomic basins of Si and H exhibit opposite signs of $\nabla^2\rho$. Such interactions have been classified as "intermediate interactions" (i.e., intermediate between closed-shell and shared interactions).[33] A similar polar covalent bond is found at the BCP between Si and C in **3c**.

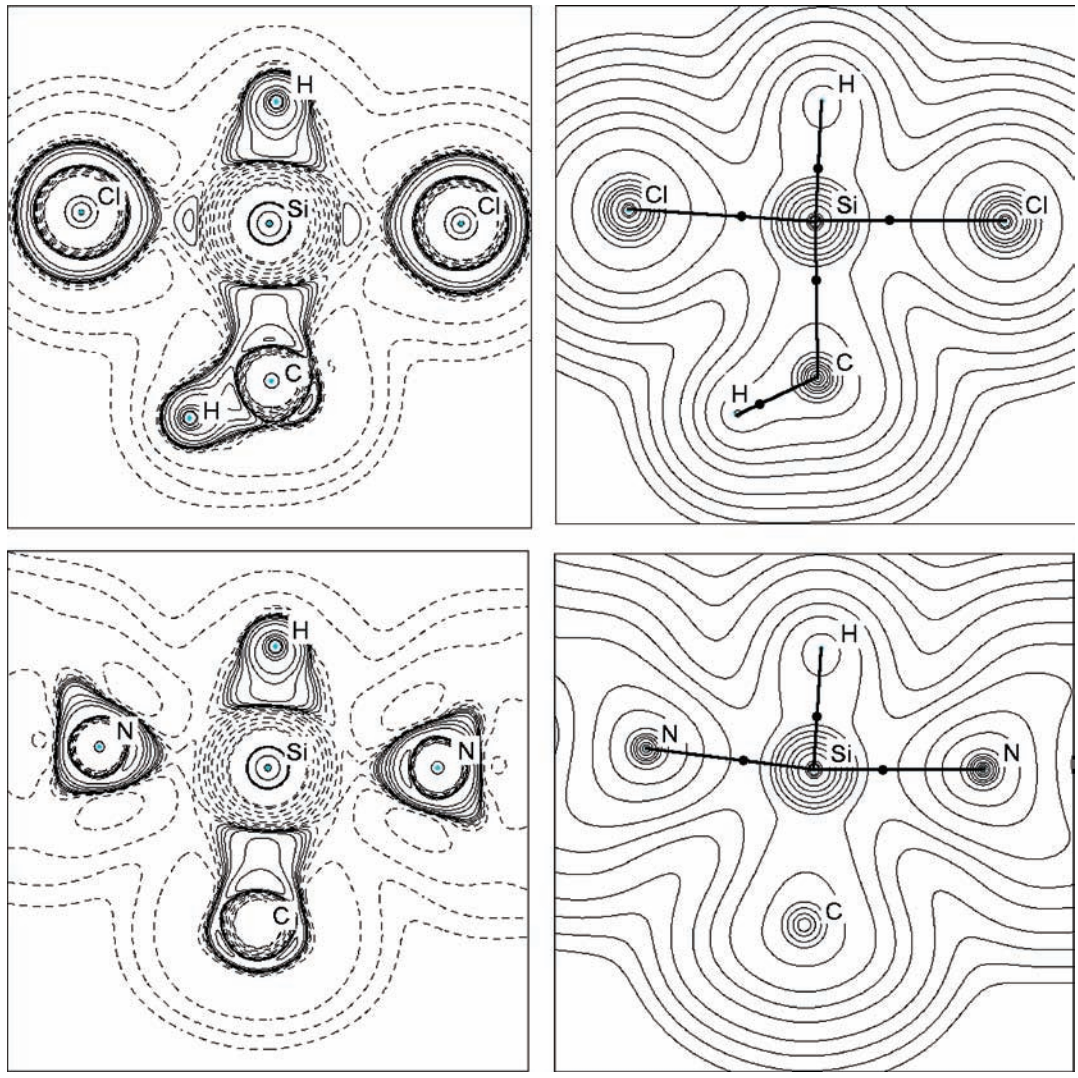

Figure 8. Representation of topological properties of **3c** in different planes: (top) $HSiCl_2C$; (bottom) $HSiN_2$. It should be noted that the carbon atom at the bottom of the $HSiCl_2C$ graphics lies outside this plane. (left) Laplacian of the electron density. Positive values of $\nabla^2\rho$ are drawn with dashed lines and represent regions of charge depletion; negative values of $\nabla^2\rho$ are drawn with solid lines and represent regions of charge concentration. (right) Electron density. Selected bond paths and BCPs are drawn on the figures. The contour values for both representations in atomic units are 0.001, 0.002, 0.004, 0.008, 0.02, 0.04, 0.08, 0.2, 0.4, 0.8, 2, 4, 8, 20, 40, 80, 200, 400, and 800.

A comparable bonding situation has been found in pyridine adducts of H_2SiCl_2.[5,8] Also, an experimental charge density study in combination with topological analyses revealed the presence of predominately ionic bonding in silicon complexes with a $[SiO_2N_2F_2]$ coordination framework.[37]

Natural charges in **1c**, **3c**, and selected reference molecules are shown in Table 4. The positive charge of the silicon atoms increases upon complex formation. Such an effect was discussed previously for antimony, tin, and other silicon complexes.[8,38−40] The negative charge of the pyridine nitrogen atom also increases upon complex formation. Furthermore, the chlorine and hydrogen atoms also bear higher negative charges in the complexes **1c** and **3c** than in the tetravalent molecules $HSiCl_3$ and $MeSiHCl_2$. These changes in the charge distribution provide evidence that the bonding situation in the complex involves bonds that are generally more polar than those in the educt molecules (i.e., the respective tetracoordinate silanes).

Table 4. Natural Charges of Atoms in **1c**, **3c**, and Selected Reference Molecules

	pyridine	$HSiCl_3$	**1c**	$HSiMeCl_2$	**3c**
Si		1.23	1.34	1.36	1.46
H		−0.16	−0.25	−0.18	−0.23
C				−1.25	−1.24
Cl		−0.36	−0.52[a,c]	−0.39	−0.56[a]
Cl			−0.46[b]		−0.58[b]
N	−0.46		−0.57		−0.55

[a] Chlorine without hydrogen contacts. [b] Chlorine with hydrogen contacts. [c] Average values.

Conclusions

It is possible to prepare pyridine adducts of $HSiCl_3$ and $HSiCl_2Me$ at low temperatures. Except for compound **1b**, the products are obtained in yields >95% and are stable under inert

(37) Kocher, N.; Henn, J.; Gostevskii, B.; Kost, D.; Kalikhman, I.; Engels, B.; Stalke, D. *J. Am. Chem. Soc.* **2004**, *126*, 5563–5568.
(38) Hensen, K.; Stumpf, T.; Bolte, M.; Näther, C.; Fleischer, H. *J. Am. Chem. Soc.* **1998**, *120*, 10402–10408.
(39) Fleischer, H. *Eur. J. Inorg. Chem.* **2001**, 393–404.
(40) Poleshchuk, O. K. H.; Shevchenko, E. L.; Branchadell, V.; Lein, M.; Frenking, G. *J. Quantum Chem.* **2005**, *101*, 869–877.
(41) Löwer, R.; Vongehr, M.; Marsmann, H. C. *Chem.-Ztg.* **1975**, *99*, 33.

atmosphere at room temperature. The octahedral complexes of $HSiCl_3$ are susceptible to dismutation reactions in polar solvents. In contrast, $HSiCl_2Me(Rpy)_2$ adducts do not undergo dismutation under comparable conditions, but they tend to dissociate more easily because of the reduced Lewis acidity of the Si atom. The ^{29}Si CP/MAS spectra in combination with quantum chemical calculations show that the lowest shielding is along the Cl−Si−Cl axis. The other two components of the shielding tensor (with nearly equal values for $HSiCl_3$ adducts) are aligned along the N−Si−N and H−Si−Cl/Me axes. According to the QTAIM analyses of **1c** and **3c**, the interaction between Si and Cl is predominantly ionic. This applies to the Si−N interaction as well, although distinct features of a donor−acceptor interaction do appear. The Si−H and Si−C bonds should be denoted as polar covalent. The natural charges of the atoms support the view of highly ionic bonding between silicon and its surrounding ligands.

(42) (a) Alborta, I.; Rozas, I.; Elguero, J. *J. Phys. Chem. A* **2001**, *105*, 743–749. (b) Callomon, J. H.; Hirota, E.; Kuchitsu, K.; Lafferty, W. J.; Maki, A. G.; Poete, C. S.; Buck, I.; Starck, B. In *Landolt-Börnstein New Series II, Volume 7*; Hellwege, K.-H., Hellwege, A. M., Eds.; Springer: Berlin, 1976. (c) Callomon, J. H.; Hirota, E.; Iijima, T.; Kuchitsu, K.; Lafferty, W. J.; Mez-StarckB.; Mutter, R. In *Landolt-Börnstein New Series II, Volume 15*; Hellwege, K.-H., Hellwege, A. M., Eds.; Springer: Berlin: 1987. (d) Hirota, E.; Iijima, T.; Kuchitsu, K.; Lafferty, W. J.; Ramsay, D. A.; Vogt, J. In *Landolt-Börnstein New Series II, Volume 21*; Madelung, O., Ed.; Springer: Berlin, 1992.
(43) Donald, K. J.; Böhm, M. C.; Lindner, H. J. *THEOCHEM* **2005**, *713*, 215–226.
(44) Brehm, M.; Ault, B. S. *J. Mol. Struct.* **2003**, *649*, 95–103.
(45) Endo, K.; Takeo, H.; Matsumura, C. *Bull. Chem. Soc. Jpn.* **1977**, *50*, 626–630.
(46) Herzfeld, J.; Berger, A. E. *J. Chem. Phys.* **1980**, *73*, 6021–6030.

Many reactions of (hydrido)chlorosilanes are catalyzed by pyridine bases. The presented results provide a basis for better control of these reactions, especially chlorine substitution, dismutation, and hydrosilylation. First results in the latter direction will be published soon. Furthermore, our results might help in the development of better understanding and design of suitable catalysts for the dismutation of $HSiCl_3$ to generate SiH_4 and for the hydrogenation of $SiCl_4$, both of which currently are highly attractive routes for an economical fabrication of solar-grade silicon in bulk or thin-film forms.

Acknowledgment. The German Research Foundation (Deutsche Forschungsgemeinschaft, DFG, Bonn), the TU Bergakademie Freiberg, and the German Academic Exchange Service (Deutscher Akademischer Austauschdienst, DAAD, Bonn) are acknowledged for financial support of this research.

Supporting Information Available: Further details of the experimental procedures, X-ray structure analysis data, complete author list for ref 10, and CIF files for **1f**, **1h**, **3c**, and **3g**. This material is available free of charge via the Internet at http://pubs.acs.org. The supplementary crystallographic data for this paper have also been deposited with the Cambridge Crystallographic Data Centre (CDCC) under accession codes CCDC-660038 (**1f**), CCDC-689841 (**1h**), CCDC-689840 (**3c**) and CCDC-689842 (**3g**). Copies of the data can be obtained free of charge from the CCDC, 12 Union Road, Cambridge CB2 1EZ, U.K., via www.ccdc.cam.ac.uk/data_request/cif, fax (international) at 44−1223/336−033, or e-mail at deposit@ccdc.cam.ac.uk.

JA901053W